JCB Article

Cbfa1-independent decrease in osteoblast proliferation, osteopenia, and persistent embryonic eye vascularization in mice deficient in Lrp5, a Wnt coreceptor

Masaki Kato,[1] Millan S. Patel,[2] Regis Levasseur,[2] Ivan Lobov,[4] Benny H.-J. Chang,[1] Donald A. Glass II,[2] Christine Hartmann,[5] Lan Li,[1] Tae-Ho Hwang,[1] Cory F. Brayton,[3] Richard A. Lang,[4] Gerard Karsenty,[2] and Lawrence Chan[1]

[1]Department of Molecular and Cellular Biology and Medicine, [2]Department of Molecular and Human Genetics, and [3]Department Pathology, Baylor College of Medicine, Houston, TX 77030
[4]Division of Developmental Biology, Department of Ophthalmology, Children's Hospital Research Foundation, University of Cincinnati, Cincinnati, OH 45229
[5]Department of Genetics, Harvard Medical School, Boston, MA 02115

The low-density lipoprotein receptor–related protein (Lrp)-5 functions as a Wnt coreceptor. Here we show that mice with a targeted disruption of *Lrp5* develop a low bone mass phenotype. In vivo and in vitro analyses indicate that this phenotype becomes evident postnatally, and demonstrate that it is secondary to decreased osteoblast proliferation and function in a *Cbfa1*-independent manner. *Lrp5* is expressed in osteoblasts and is required for optimal Wnt signaling in osteoblasts. In addition, Lrp5-deficient mice display persistent embryonic eye vascularization due to a failure of macrophage-induced endothelial cell apoptosis. These results implicate Wnt proteins in the postnatal control of vascular regression and bone formation, two functions affected in many diseases. Moreover, these features recapitulate human osteoporosis-pseudoglioma syndrome, caused by *LRP5* inactivation.

Introduction

The low-density lipoprotein receptor (LDLR)* gene family encodes cell surface receptors conserved from *Caenorhabditis elegans* to humans (Hussian et al., 1999; Willnow, 1999; Herz and Beffert, 2000) that are characterized by the presence of cysteine-rich complement-type LDLR ligand-binding domains (Herz and Beffert, 2000). There are at least ten members of the LDLR gene family in mammals, and five of these (LDLR, very low-density lipoprotein receptor, apolipoprotein E receptor-2, LDLR-related protein [LRP]-1, and megalin) recognize apolipoprotein E as one of their ligands. Five other LRPs have been described: LRP3 (Ishii et al., 1998); LRP4 (Tomita et al., 1998); LR11 (Yamazaki et al., 1996); LRP5 (Dong et al., 1998; Hey et al., 1998; Kim et al., 1998); and LRP6 (Brown et al., 1998). Although the ligands for most of these receptors are unknown, recent studies in *Drosophila* have identified a class of ligands for Lrp5 and Lrp6, and thereby a signaling pathway in which they act.

In *Drosophila*, arrow encodes a single-pass transmembrane protein thought to act as a coreceptor for wingless, as inactivation of arrow results in a wingless-like phenotype (Wehrli, 1999). Arrow is an LRP strikingly homologous to vertebrate LRP5 and LRP6 (Wehrli, 1999; Pinson et al., 2000; Tamai et al., 2000). This sequence homology is consistent with the multiple Wnt deficiency–like phenotypes of Lrp6-deficient mice (Pinson et al., 2000). Lrp5, the other homologue of arrow and a close relative of Lrp6, is involved in Wnt signaling in vitro. Indeed, in NIH3T3 fibroblasts, the interaction of Lrp5 with Axin is initiated by Wnt treatment of these cells

The online version of this article contains supplemental material.

Address correspondence to Gerard Karsenty or Lawrence Chan, Baylor College of Medicine, One Baylor Plaza, Rm. S921, Houston, TX 77030. Tel.: (713) 798-4490. Fax: (713) 798-1530.
E-mail: karsenty@bcm.tmc.edu or lchan@bcm.tmc.edu

M. Kato, M.S. Patel, R. Levasseur, Ivan Lobov, and B.H.-J. Chang contributed equally to this work.

*Abbreviations used in this paper: BFR, bone formation rate; BrdU; 5-bromo-2′-deoxy-uridine; dpc, days postcoitum; ECM, extracellular matrix; ES, embryonic stem; LDLR, low-density lipoprotein receptor; Lrp, LDLR-related protein; MAR, matrix apposition rate; PM, pupillary membrane; TRAP, tartrate-resistant acid phosphatase; TVL, tunica vasculosa lentis.

Key words: low bone mass; blindness; Wnt; osteoblast function; vascular regression

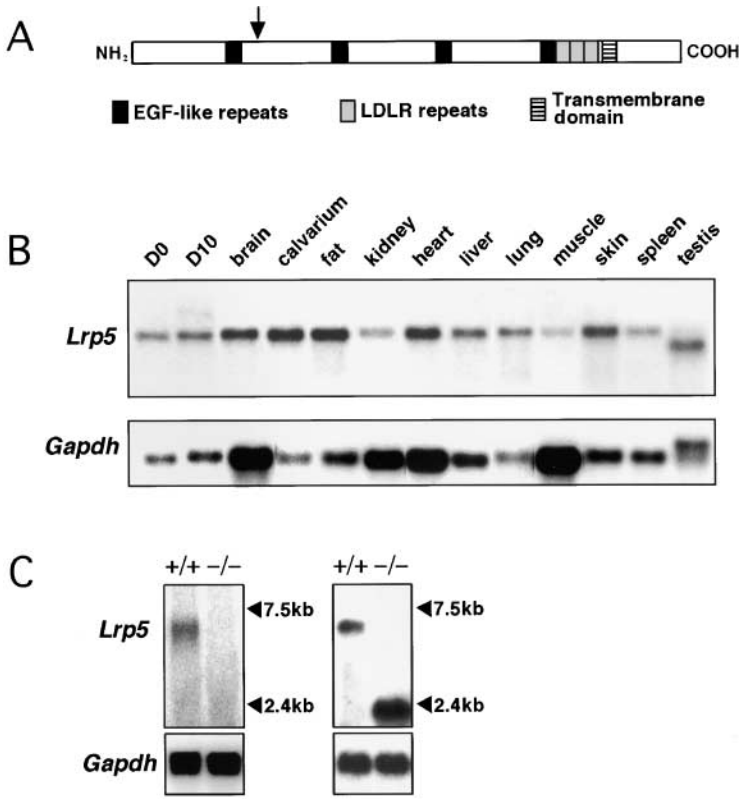

Figure 1. **Targeted disruption of *Lrp5***. (A) Structure of the Lrp5 protein and location of targeted disruption of *Lrp5* (vertical arrow). (B) Northern blot analysis showing a broad pattern of *Lrp5* expression. *Gapdh* was used as a control for RNA integrity. (C) Northern blot analysis showing no Lrp5 transcript in $Lrp5^{2/2}$ animals using a 39 probe (left) and the presence of a truncated transcript when using a 59 probe (right).

(Mao et al., 2001). The observation that overexpression of *Lrp6*, but not of *Lrp5*, induced dorsal axis duplication in *Xenopus* (Tamai et al., 2000) indicates that these two receptors control different functions, presumably by interacting with distinct ligands of the Wnt family.

The Wnt proteins are secreted proteins that control multiple developmental processes including mesoderm induction, cell fate determination, limb patterning, and organogenesis (Parr and McMahon, 1998; Wodarz and Nusse, 1998; Vainio et al., 1999; Hartmann and Tabin, 2001). Wingless in *Drosophila* and Wnt proteins in vertebrates initiate these events by binding to seven transmembrane domain receptors of the Frizzled family (Bhanot et al., 1996; Wodarz and Nusse, 1998). Wnt binding to Frizzled results in stabilization of β-catenin, which then interacts with transcription factors of the Lef/Tcf family to activate specific gene expression programs (Huelsken and Birchmeier, 2001). Distinct Wnt proteins control early events during skeletal development such as limb patterning (Perrimon and McMahon, 1998) and joint formation (Hartmann and Tabin, 2001). However, the recent findings that *LRP5* is inactivated in osteoporosis-pseudoglioma syndrome patients (Gong et al., 2001) and is mutated in patients with the high bone mass syndrome (Little et al., 2002) strongly suggest that Wnt proteins may control other aspects of skeletal biology later during development and postnatally.

Through the analysis of mice lacking most of the Lrp5 protein we present evidence that the Lrp5 signaling pathway is required for osteoblast proliferation as well as for bone matrix deposition by differentiated osteoblasts. Surprisingly, these phenotypic abnormalities occur in the context of normal *Cbfa1/Runx2* (*Cbfa1*) expression, a gene usually viewed as controlling osteogenesis (Karsenty, 1999). Thus, these results suggest a role for Cbfa1-independent pathways in the control of osteoblast proliferation and function. Biochemical and expression evidence indicates that Lrp5 binds directly to Wnt proteins and is required for optimal signaling of a distinct subset of Wnt proteins belonging to the Wnt1 subfamily in osteoblasts. Lrp5 is also necessary for the normal regression of embryonic vasculature in the eye. Together, these results demonstrate that the Lrp5 signal transduction pathway, and thereby Wnt proteins, regulate osteoblast proliferation, function, and eye vascularization during late development and after birth.

Results

Generation of $Lrp5^{-/-}$ mice

Lrp5 encodes a 1,614-amino acid transmembrane protein with an extracellular domain containing EGF-like and LDLR domains, a small transmembrane domain, and an intracellular domain (Fig. 1 A). *Lrp5* is very broadly expressed (Fig. 1 B). To inactivate *Lrp5* in mice, we generated an allele that disrupts the extracellular domain, resulting in a truncated polypeptide due to the insertion of an IRES-*LacZ-Neomycin* cassette at amino acid 373 (Fig. S1, A and B). A very similar mutation is found in human patients and results in the same phenotypic consequences as those observed with a complete deletion of the gene (Gong et al., 2001).

Chimeras generated from two independent targeted clones transmitted the mutation through the germ line, and the phenotypic abnormalities described below were observed in mutant mice derived from both of these targeted clones. Northern blot analysis of liver RNA failed to detect *Lrp5* ex-

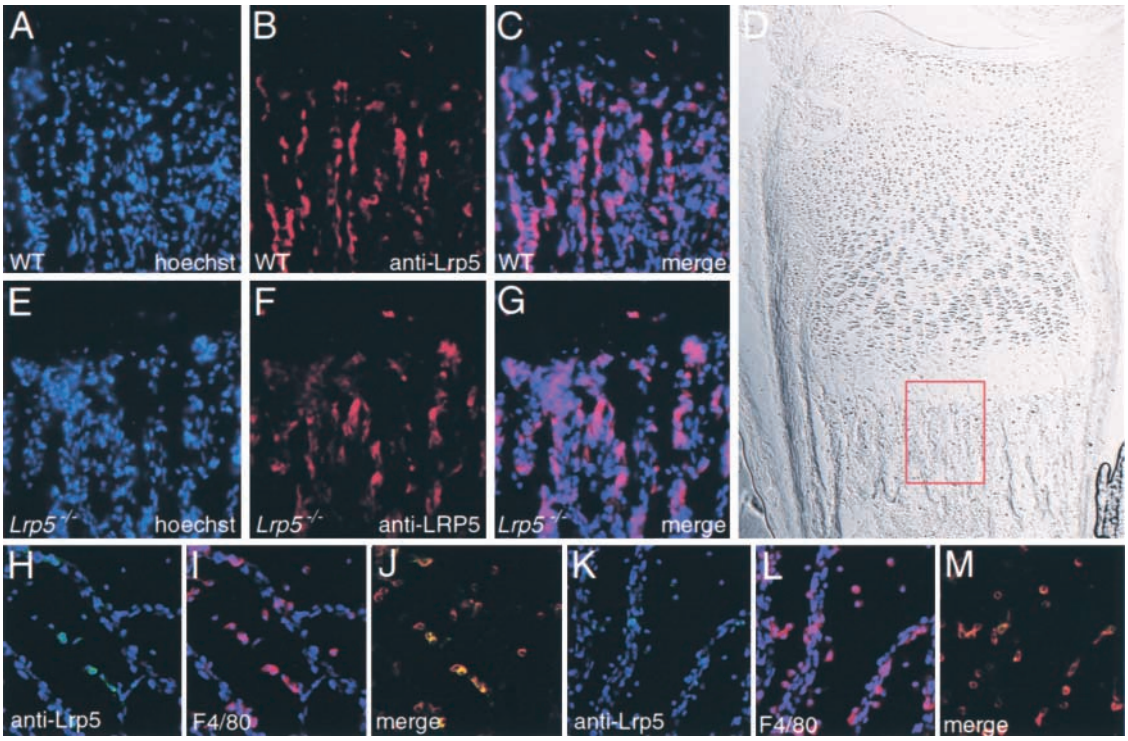

Figure 2. **Lrp5 expression in osteoblasts and ocular macrophages.** (A–C) Lrp5 expression in osteoblasts and bone lining cells in the primary spongiosa of the femur in wild-type mice. (A) Hoechst nuclear staining is shown in blue; (B) Anti-Lrp5 immunoreactivity in red. (C) A merge of the red and blue channels. (D) DIC image of distal femur from wild-type with a box showing the region examined in A–C. (E–G) Lrp5 expression in the primary spongiosa of the femur in $Lrp5^{-/-}$ mice. (E) Hoechst nuclear staining. (F) Anti-Lrp5 immunoreactivity. (G) Merge. (H–M) Whole-mount preparations of hyaloid vessels from wild-type (H–J) and $Lrp5^{-/-}$ (K–M) mice. (H and K) Immunoreactivity for Lrp5. (I and L) Immunoreactivity with the macrophage-specific antibody F4/80, both with Hoechst nuclear staining. (J and M) Merge of the red, blue, and green channels; yellow cells indicate that macrophages are positive for Lrp5.

pression in $Lrp5^{-/-}$ mice (Fig. S1 C, left) when using a probe derived from exons 10 to 12, indicating that the disrupted exon 6 is not being skipped by the splicing machinery to recreate a near normal transcript. Using a 5′ probe derived from exons 1 and 2 we could detect a truncated transcript in $Lrp5^{-/-}$ mice (Fig. S1 C, right). Immunohistochemistry demonstrated the presence of the truncated polypeptide in osteoblasts (Fig. 2).

Heterozygous ($Lrp5^{+/-}$) mice appeared phenotypically normal. Crosses between heterozygotes produced litters of normal size, and Southern blot analysis revealed that $Lrp5^{-/-}$ mice were recovered at close to the expected Mendelian ratio (Fig. S1 C). $Lrp5^{-/-}$ mice had a normal morphological appearance and were viable and fertile, although a small but significant number of them died within the first month of life, presumably after fractures (see below). The penetrance and the severity of the two phenotypes described below were identical on a C57BL/6Jx129/SvEv or a 129/SvEv genetic background.

Immunolocalization of Lrp5

To identify the cell types producing Lrp5, we used an antibody directed against the amino terminal part of the molecule which is still transcribed in $Lrp5^{-/-}$ mice (Figueroa et al., 2000). By immunohistochemistry we observed the presence of the protein in osteoblasts lining the endosteal and trabecular bone surfaces (Fig. 2, A–G). We could not detect any expression in osteoclasts (unpublished data). Lrp5 protein was detected only in F4/80-positive macrophages found closely associated with the vitreous microvasculature of the eye (Fig. 2, H–M). Consistent with its broad pattern of RNA expression, Lrp5 was also detected in other tissues including liver, pancreas, skin, and brain (Figueroa et al., 2000; unpublished data).

Low bone mass phenotype in $Lrp5^{-/-}$ mice

A small number of mutant animals were limping while walking, suggesting the existence of a skeleton-related abnormality. Radiographic analysis of one of these mutant mice at 2 mo of age revealed the presence of a fracture in the tibia betraying the existence of a low bone mass phenotype (Fig. S2) that was present in all $Lrp5^{-/-}$ mice at that age (Fig. 3 A; unpublished data).

Histological analysis of the skeleton of 2-mo-old $Lrp5^{-/-}$ mice revealed a significant decrease in bone volume compared to wild-type littermates, and this low bone mass phenotype was observed in all mutant animals analyzed regardless of sex and at all stages analyzed (Fig. 3 B; unpublished data). In particular, analysis of mice at 2 wk of age revealed a marked decrease in the quantity of mineralized bone in the primary spongiosa of $Lrp5^{-/-}$ mice (Fig. 3 C). As a result, mutant mice fail to acquire as much bone as wild-type littermates early during life, and their bone mass remains lower throughout life (Fig. 3 D). Serum and urine levels of cal-

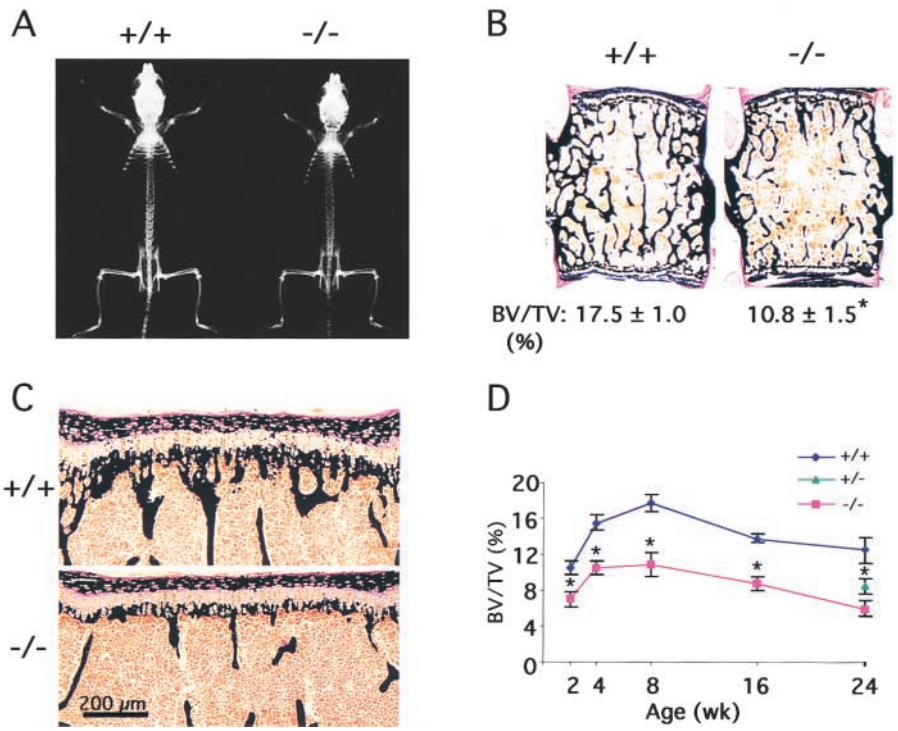

Figure 3. **Low bone mass in *Lrp5*$^{-/-}$ mice.** (A) Radiograph of the whole body of 2 mo-old wild-type and *Lrp5*$^{-/-}$ mice showing decreased lucency of the entire *Lrp5*$^{-/-}$ skeleton. (B) Histological analysis of vertebrae from 2-mo-old wild-type and *Lrp5*$^{-/-}$ mice showing low bone mass in the mutant mice. (C) Histological analysis of vertebrae from 2-wk-old wild-type and *Lrp5*$^{-/-}$ mice showing a decreased number of trabeculae in the primary spongiosa of *Lrp5*$^{-/-}$ mice. (D) *Lrp5*$^{-/-}$ mice have a lower bone mass throughout life. Green triangle indicates a significantly lower bone mass in *Lrp5*$^{+/-}$ mice. Asterisks indicate a statistically significant difference between two groups of mice ($P < 0.05$). Error bars represent SD.

cium and phosphate were normal in *Lrp5*$^{-/-}$ mice, indicating that the low bone mass phenotype was not due to a metabolic perturbation (Table 1).

Osteoporosis-pseudoglioma, a rare syndrome caused by inactivating mutations in *LRP5* in humans (Gong et al., 2001), is usually viewed as an autosomal recessive disease (Gong et al., 1996). However, because two obligate heterozygote individuals had severe osteoporosis (Superti-Furga et al., 1986), we studied the bones of *Lrp5*$^{+/-}$ mice. As shown in Fig. 3 D, 6-mo-old *Lrp5*$^{+/-}$ mice had a significantly lower bone volume than their wild-type littermates, indicating that this is a dominant phenotype. That the low bone mass phenotype was noticeably more severe in *Lrp5*$^{-/-}$ mice than in *Lrp5*$^{+/-}$ mice reinforces the notion that the engineered mutation is a loss-of-function mutation.

Decreased bone formation postnatally in *Lrp5*$^{-/-}$ mice

The cellular basis of this low bone mass phenotype was studied using histomorphometric analyses and biochemical and cell-based assays. The bone formation aspect of bone remodeling was analyzed by measuring the bone formation rate (BFR), an indicator of osteoblast activity, after in vivo double labeling with calcein, a marker of newly formed bone. In 6-mo-old *Lrp5*$^{-/-}$ mice there was a twofold decrease in the BFR compared with wild-type littermates (Fig. 4 A). A similar difference was observed in 2- and 4-mo-old *Lrp5*$^{-/-}$ mice (unpublished data). The decreased BFR was solely due to a decreased matrix apposition rate (MAR) (Fig. 4 A, arrow), an index of the amount of bone matrix deposited per osteoblast cluster (0.75 ± 0.05 vs. 0.45 ± 0.06 μm/d; $P < 0.05$) (Aaron et al., 1984). This decreased MAR directly demonstrates a functional defect of osteoblasts in vivo in the absence of Lrp5. Consistent with the dominant nature of the osteoporosis-like phenotype, the BFR was also significantly decreased in *Lrp5*$^{+/-}$ mice (88.6 ± 4.8 vs. 60.5 ± 3.9 $\mu m^3/\mu m^2/y$; $P < 0.05$). We also performed osteoblast counts in the primary and secondary spongiosa. The results obtained were identical in both cases: total osteoblast number per bone area was significantly decreased in *Lrp5*$^{-/-}$ mice (Fig. 4 B). To further study osteoblast function, we assayed the ability of primary osteoblast cultures to mineralize an extracellular matrix (ECM). As shown in Fig. 4 C, mineralization of the ECM surrounding *Lrp5*$^{-/-}$ osteoblasts was delayed compared with what we observed in wild-type osteoblasts at day 10 of culture. This latter finding supports the notion that *Lrp5*$^{-/-}$ osteoblasts have a functional defect. However, it may alternatively be explained by the abnormal proliferation of *Lrp5*$^{-/-}$ osteoblasts (see below). The growth plate of *Lrp5*$^{-/-}$ mice appeared normal, indicating that chondrogenesis was not overtly affected (Fig. 4 D).

To define the earliest time point when the bone phenotype of the *Lrp5*$^{-/-}$ mice could be detected we stained skeletal preparations of 17.5 d postcoitum (dpc) embryos, newborn, and 4-d-old (P4) wild-type and *Lrp5*$^{-/-}$ mice with Alizarin red/Alcian blue. Alcian blue stains proteoglycan-rich cartilage ECM, whereas Alizarin red stains mineralized

Table I. **Serum and urine calcium and phosphate concentrations**

Analyte	Genotype	Mean	SD
Serum calcium (mg/dl)	+/+	9.58	0.41
	−/−	9.53	1.15
Serum phosphate (mg/dl)	+/+	6.84	0.47
	−/−	7.38	1.75
Urine calcium:creatinine	+/+	1.09	0.94
	−/−	1.04	0.18
Urine phosphate:creatinine	+/+	45.9	11.4
	−/−	33.1	25.7

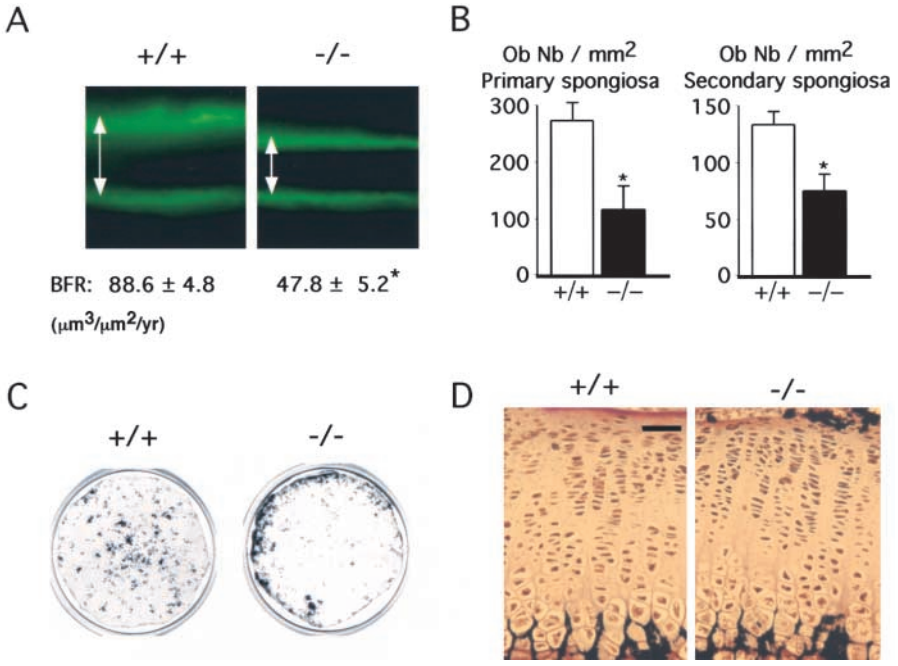

Figure 4. **Functional defect in *Lrp5*$^{-/-}$ osteoblasts.** (A) Calcein double labeling in 6-mo-old wild-type and *Lrp5*$^{-/-}$ mice. The distance between the two labels (double-headed arrows) represents the MAR which is decreased in *Lrp5*$^{-/-}$ mice. As a result, the BFR is significantly lower in *Lrp5*$^{-/-}$ mice. (B) Decreased osteoblast number per bone area in the primary (left) and secondary (right) spongiosa of *Lrp5*$^{-/-}$ mice compared with wild-type. (C) Delayed mineralization in primary *Lrp5*$^{-/-}$ osteoblast cultures compared with wild-type cultures at day 10 of mineralization. (D) Normal tibial growth plate in 2-mo-old *Lrp5*$^{-/-}$ mice (von Kossa stain). Asterisks indicate a statistically significant difference between two groups of mice ($P < 0.05$). Error bars represent SD.

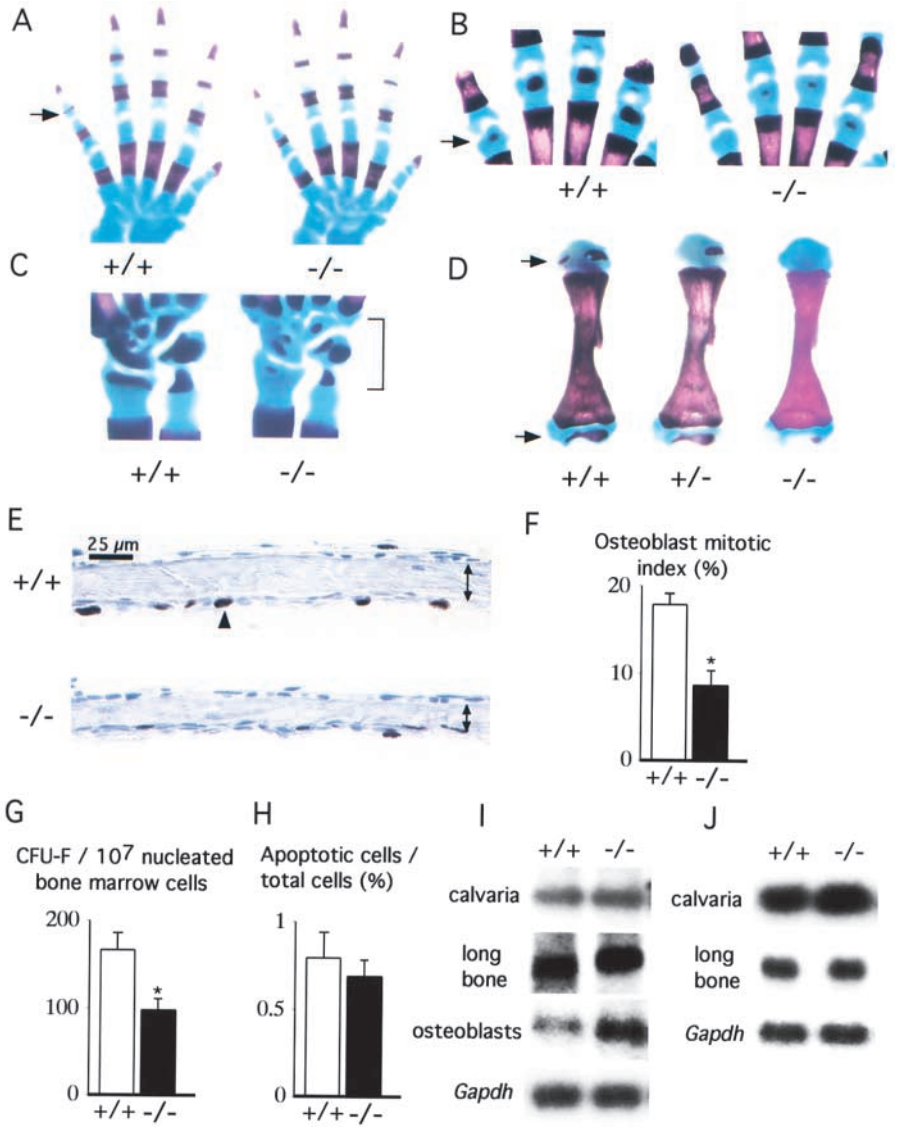

Figure 5. **Postnatal onset of the bone phenotype in *Lrp5*$^{-/-}$ mice.** (A) Subtle delay of fifth middle phalanx ossification in newborn *Lrp5*$^{-/-}$ mice. (B) Delayed ossification of metacarpals. (C) Carpals (bracket). (D) Humeri in 4-d-old *Lrp5*$^{-/-}$ mice. Arrows in A, B, and D indicate ossification centers. A subtle delay was also evident in 44% (8/18) of heterozygote mice (D, middle). (E) Sections of calvaria from 4-d-old mice showing a decreased number of BrdU-positive cells (arrowhead) in *Lrp5*$^{-/-}$ mice compared with wild-type littermates. Double-headed arrows indicate the greater thickness of wild-type calvarium. (F) Osteoblast mitotic index (percentage of BrdU-positive cells per total cell number) in wild-type and *Lrp5*$^{-/-}$ mice ($n = 8$ per genotype). (G) Quantification of alkaline phosphatase positive stromal cell progenitors (CFU-F) in the bone marrow of wild-type and *Lrp5*$^{-/-}$ mice ($n = 9$ mice per genotype). (H) Quantification of apoptotic cells by TUNEL assay in wild-type and *Lrp5*$^{-/-}$ mice ($n = 5$ per genotype). (I) Northern blot analysis of *Cbfa1* expression in wild-type and *Lrp5*$^{-/-}$ calvaria, long bones and primary osteoblasts. (J) Northern blot analysis of *Osteocalcin* expression in wild-type and *Lrp5*$^{-/-}$ calvaria and long bones. (I and J) *Gapdh* expression level was used as a loading control; results are representative of three samples ($n = 3$ mice per sample). Asterisks indicate a statistically significant difference between two groups of mice ($P < 0.05$). Error bars represent SD.

ECM. There was no ossification defect in any skeletal element in 17.5 dpc *Lrp5*$^{-/-}$ embryos (unpublished data). In contrast, in newborn *Lrp5*$^{-/-}$ mice, a subtle delay in osteogenesis could be observed in the digits as shown by the absence of the fifth middle phalangeal ossification center (Fig. 5 A, arrow). In 4-d-old mutant mice, the delay in osteogenesis became more pronounced and ossification centers of the wrist, distal metacarpal bones, femora, humeri, and ulnae that stained red in wild-type mice were absent or smaller in *Lrp5*$^{-/-}$ mice (Fig. 5, B–D, and unpublished data). Consistent with their osteopenic phenotype, we observed a milder delay of osteogenesis in *Lrp5*$^{+/-}$ mice (Fig. 5 D). Collectively, these data demonstrate that skeletal development appears to proceed normally until 17.5 dpc, after which osteogenesis and bone formation become hampered.

The bone resorption aspect of bone remodeling was first analyzed by measuring urinary elimination of deoxypyridinoline crosslinks (Dpd), a biochemical marker of bone resorption, and the number of osteoclasts. Both parameters were identical in wild-type and mutant mice (urine Dpd/creatinine ratio 10.3 ± 2.1 in wild-type mice vs. 11.0 ± 6.2 in *Lrp5*$^{-/-}$ mice). We also assayed for the ability of spleen and bone marrow precursor cells to differentiate into tartrate-resistant acid phosphatase (TRAP)-positive osteoclasts in vitro, as well as their ability to resorb bone in vitro, and we did not observe any difference between wild-type and *Lrp5*$^{-/-}$ cells (unpublished data). Taken together, these data indicate that bone resorption is not overtly affected in *Lrp5*$^{-/-}$ mice.

Abnormal osteoblast proliferation and normal *Cbfa1* expression in *Lrp5*$^{-/-}$ mice

The perinatal onset of the osteogenesis defect, along with the decreased number of osteoblasts in *Lrp5*$^{-/-}$ mice, suggested that *Lrp5* could be required for osteoblast proliferation and/or differentiation. To determine if osteoblast proliferation was affected, we measured the number of cells actively synthesizing DNA by 5-bromo-2′-deoxy-uridine (BrdU) incorporation in vivo. Fig. 5 E shows sections of calvaria from 4-d-old wild-type and *Lrp5*$^{-/-}$ mice. Significantly fewer labeled nuclei were detected in sections from *Lrp5*$^{-/-}$ mice compared to those derived from wild-type mice (Fig. 5 E). The total number of osteoblasts was also decreased in *Lrp5*$^{-/-}$ calvaria but even after correction for this decreased cell number there was still a significantly lower mitotic index for mutant osteoblasts in vivo (Fig. 5 F). To assess whether this proliferation defect extended to progenitors of the osteoblast lineage, we determined the number of stromal cell progenitors (CFU-F) in wild-type and *Lrp5*$^{-/-}$ bone marrow. The numbers of nucleated bone marrow cells obtained from wild-type and *Lrp5*$^{-/-}$ bone marrow were similar (unpublished data). However, as shown in Fig. 5 G, *Lrp5*$^{-/-}$ bone marrow cells formed almost twofold fewer alkaline phosphatase–positive colonies than wild-type bone marrow cells, suggesting the existence of an early proliferation defect in the osteoblast lineage. There was no increased apoptosis in the calvaria of *Lrp5*$^{-/-}$ mice (Fig. 5 H), indicating that the low mitotic index of mutant osteoblasts was solely due to a proliferation defect.

To determine if the osteoblast phenotype affected the classical Cbfa1 pathway controlling osteoblast differentiation we examined the expression of *Cbfa1* in calvaria, long bones, and primary osteoblasts. As shown in Fig. 5 I, *Cbfa1* expression was not decreased in the absence of Lrp5, indicating that this bone phenotype develops in a Cbfa1-independent manner. Because there are fewer osteoblasts in *Lrp5*$^{-/-}$ calvaria and long bones, it is possible that Cbfa1 may be upregulated in these mice. Moreover, the normal expression of *Osteocalcin* in *Lrp5*$^{-/-}$ (Fig. 5 J) mice suggests also that osteoblast differentiation is not affected in the absence of Lrp5.

In summary, in vivo and cell-based assays support the hypothesis that the low bone mass phenotype observed in *Lrp5*$^{-/-}$ mice is due to two main defects, both occurring in a *Cbfa1*-independent manner: a decrease in osteoblast proliferation evidenced by the BrdU in vivo labeling experiments, and a decrease in bone matrix deposition shown by the decreased BFR.

Lrp5 acts as a Wnt receptor in osteoblasts

The homology between arrow, a coreceptor for wingless in *Drosophila*, and Lrp5, as well as the requirement of Lrp5 for Wnt signaling in NIH3T3 fibroblasts (Wehrli, 1999; Mao et al., 2001), suggested that the bone phenotype of *Lrp5*$^{-/-}$ mice may be secondary to a defect in Wnt signaling in osteoblasts.

To test this hypothesis, we first performed DNA cotransfection experiments in primary calvarial osteoblasts obtained from wild-type or *Lrp5*$^{-/-}$ 4-d-old mice. Cells were transfected with a luciferase reporter construct containing multiple copies of an oligonucleotide containing the Lef1 binding site (TOPtkluc) (Korinek et al., 1997), as well as a Lef1 expression vector. Using this assay, cotransfection of a Wnt1 expression vector consistently enhanced Lef1-dependent transcription to a higher degree in wild-type than in *Lrp5*$^{-/-}$ primary osteoblasts (Fig. 6 A). Importantly, cotransfection of an LRP5 expression vector into *Lrp5*$^{-/-}$ osteoblasts restored the ability of Wnt1 to induce Lef1-dependent gene expression to wild-type levels (Fig. 6 B).

To identify a subgroup of Wnt proteins requiring LRP5 to better transduce its signal in osteoblasts, we also performed DNA cotransfection experiments in primary osteoblasts using an expression vector for Wnt4 or a conditioned medium from cells producing soluble Wnt3a (Shibamoto et al., 1998). Soluble Wnt3a increased Lef1-dependent gene expression equally in wild-type and *Lrp5*$^{-/-}$ osteoblasts, indicating that in this assay there is no detectable signaling defect for Wnt3a in the absence of Lrp5. However, as the addition of an LRP5 expression vector further increased twofold the ability of Wnt3a to stimulate Lef1-dependent gene expression in osteoblasts, we cannot rule out the possibility that optimal Wnt3a signaling may require Lrp5 (Fig. 6 B). In contrast, Wnt4 stimulated Lef1-dependent gene expression to a lesser extent, and this was virtually not affected by the presence of LRP5 (Fig. 6 C). Western blot analyses were performed to demonstrate the presence of each protein after DNA transfection; these analyses also demonstrated the ability of LRP5 to enhance Wnt-dependent accumulation of cytosolic β-catenin levels (Figs. 6 D and S2). Coimmunoprecipitation experiments demonstrated that Wnt1 and Wnt4 are able to bind directly to LRP5 (Fig. 6 E). These results in-

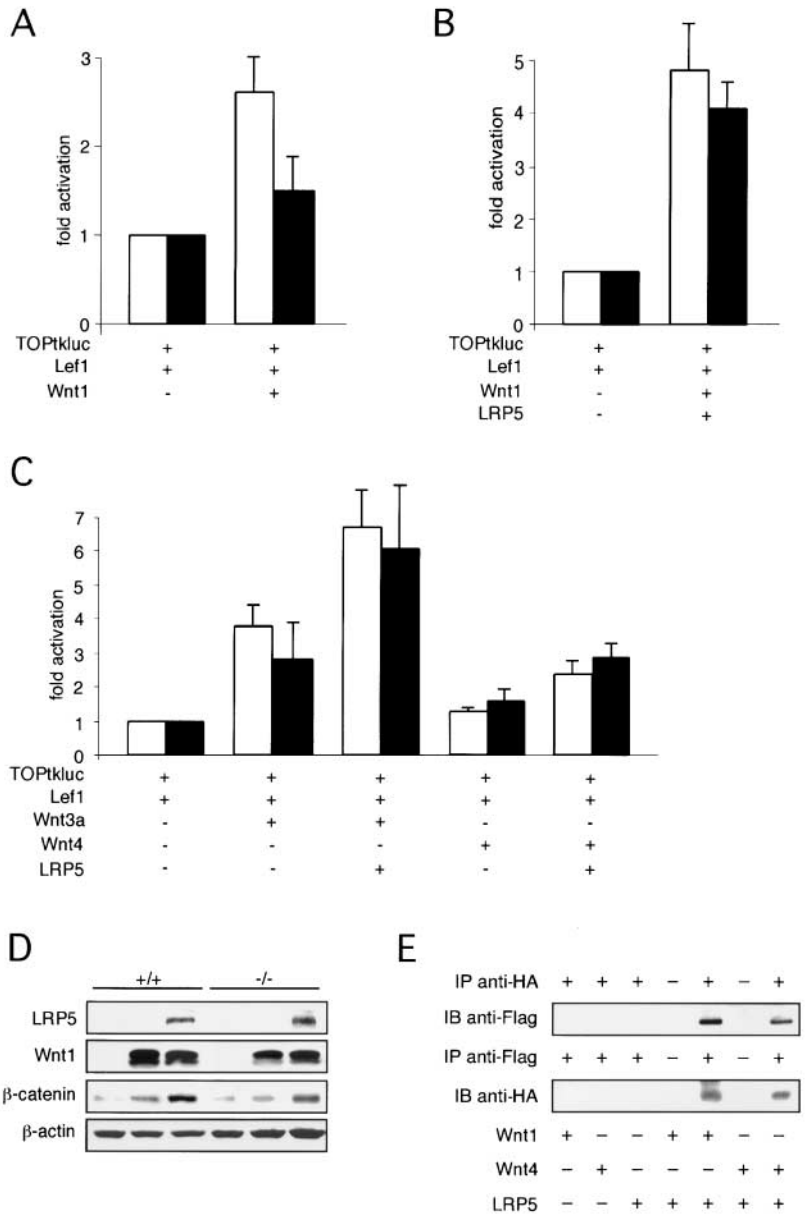

Figure 6. **LRP5-dependent activation of gene expression by Wnt proteins.** (A) Wnt1 activates Lef1-dependent gene expression in wild-type but poorly in *Lrp5*$^{-/-}$ primary osteoblasts. (B) Cotransfection of LRP5 in *Lrp5*$^{-/-}$ osteoblasts allows Wnt1 to activate Lef1-dependent gene expression to wild-type levels. (C) Cotransfection of LRP5 with Wnt3a-conditioned medium or an expression vector for Wnt4 in wild-type (white bars) and *Lrp5*$^{-/-}$ primary osteoblasts (black bars). (D) Western blot analysis to confirm expression of transfected plasmids and to demonstrate the ability of Wnt1-LRP5 cotransfection to stimulate cytoplasmic β-catenin accumulation. (E) Direct binding of LRP5 to Wnt1 or Wnt4. COS-7 cells were transfected with Flag-LRP5 and HA-Wnt1 or HA-Wnt4 as indicated. LRP5 or Wnts were immunoprecipitated from the cell lysate using anti-Flag or anti-HA antibody, subjected to SDS-PAGE and immunoblotted with anti-HA and anti-Flag antibody, respectively.

dicate that, in the conditions of this assay and among the Wnt proteins tested, Wnt1 or a related Wnt protein may be a preferred ligand for LRP5 in osteoblasts.

Expression of *Wnts,* and of genes encoding Wnt signaling molecules in bone

Lrp5 is expressed in osteoblasts at early and late stages of differentiation (Fig. 1 B). To determine if the low bone mass phenotype in the *Lrp5*$^{-/-}$ mice was consistent with the expression pattern of other molecules involved in Wnt signaling, we analyzed their expression in bone and in osteoblasts. *Wnt1* was expressed at high levels in calvaria in both wild-type and *Lrp5*$^{-/-}$ mice (Fig. 7 A). *Wnt1* expression was detected in primary osteoblasts at higher amplification levels, but was absent from day 0 *Lrp5*$^{-/-}$ osteoblasts (Fig. 7 A), suggesting that *Wnt1* expression by proliferating osteoblasts requires the presence of *Lrp5*. The normal level of *Wnt1* expression in day 10 *Lrp5*$^{-/-}$ osteoblasts suggests that Lrp5 is not necessary for *Wnt1* expression at later stages of differentiation when proliferation ceases. *Wnt4* and *14* were also expressed in calvaria and in osteoblasts in wild-type and *Lrp5*$^{-/-}$ samples (Fig. 7 B). *Wnt3a* expression was not detected in calvaria, long bones, or primary osteoblasts, regardless of the level of amplification indicating that it may not be the ligand for Lrp5 in bone (unpublished data).

The Wnt receptors *Frizzled2* and *6* were both expressed in calvaria and primary osteoblasts and their expression levels were unaffected by the lack of Lrp5 (Fig. 7 B). Because *Lef1* and *Tcf4* had previously been shown to be expressed in bone by in situ hybridization (Hartmann and Tabin, 2000), we studied the expression of these two members of the *Lef/Tcf* family of transcription factors. Both were expressed in primary osteoblasts. Interestingly *Lef1*, but not *Tcf4*, expression was markedly decreased in *Lrp5*$^{-/-}$ osteoblasts (Fig. 7 C). In summary, members of the canonical Wnt signaling pathway are present in osteoblasts and their expression is affected by *Lrp5* disruption.

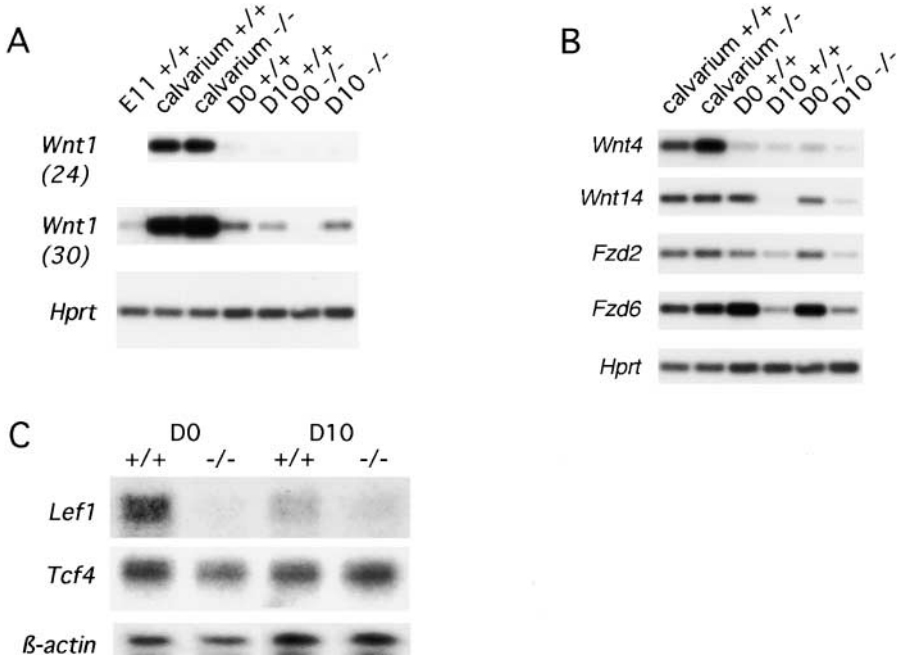

Figure 7. **Expression of *Wnts* and Wnt signaling molecules in bone.** (A) *Wnt1* is highly expressed in calvaria compared with day 11 (E11) embryos or primary osteoblasts (24 cycle RT-PCR, top). *Wnt1* expression is not present in proliferating (D0) *Lrp5*$^{-/-}$ osteoblasts (30 cycle RT-PCR, middle). (B) Wnt4, Wnt14, *Frizzled2*, and *Frizzled6* expression in calvaria and primary osteoblasts (24 cycle RT-PCR). (C) Decreased expression of *Lef1*, but not *Tcf4*, in *Lrp5*$^{-/-}$ osteoblasts determined by RNase protection assay.

Abnormal macrophage-mediated apoptosis in the eyes of *Lrp5*$^{-/-}$ mice

Postnatal development of the rodent eye involves the regression of three related vascular networks called the pupillary membrane (PM), tunica vasculosa lentis (TVL), and the hyaloid vessels (Fig. 8 A). In wild-type mice, regression of these networks is normally complete by P12 for the PM and by P16 for the TVL and hyaloid vessels (Ito and Yoshioka, 1999). Histological analysis of eyes at 6 mo of age revealed the presence of hyaloid vessels in 70% (28/40) of *Lrp5*$^{-/-}$ mice and in none of the wild-type controls. To define the onset of this phenotype, we performed a series of dissections of the capillary networks in order to compare their rates of regression. Although both the PM and TVL showed mild delays in regression (unpublished data), this response was dramatic in the hyaloid vessels; quantification of the number of capillary segments over a P3–P8 time course (Fig. 8 B) indicated that loss of segments was much slower in *Lrp5*$^{-/-}$ mice. The presence of equal numbers of capillary segments in wild-type and *Lrp5*$^{-/-}$ mice at P3 indicated that the persistence was not a trivial consequence of early vessel overgrowth in *Lrp5*$^{-/-}$ mice. The persistence of the hyaloid vessels is readily visualized when comparing histological preparations from wild-type (Fig. 8, D–F) and *Lrp5*$^{-/-}$ mice (Fig. 8, G–I) over the P3–P8 time course. Higher magnifications of hyaloid vessel preparations (Fig. 2, G–L) indicate that the number of macrophages associated with wild-type and *Lrp5*$^{-/-}$ hyaloid vessels is not different. No delay in hyaloid vessel regression was detected in *Lrp*$^{+/-}$ mice (unpublished data).

To examine the cellular basis for the lack of capillary regression in *Lrp5*$^{-/-}$ mice, we performed TUNEL analysis (Gavrieli et al., 1992) to detect apoptotic cells. Regression of the PM is known to occur on a segmental basis (Lang et al., 1994), and hyaloid vessel preparations from both wild-type and *Lrp5*$^{-/-}$ mice showed segmental TUNEL labeling consistent with this expectation (Fig. 8, D–F, wild-type, and G–I, *Lrp5*$^{-/-}$). However, quantification indicates that the proportion of TUNEL-labeled segments is lower in *Lrp5*$^{-/-}$ mice at all time points examined (Fig. 8 C). Furthermore, in the wild-type, the proportion of apoptotic segments increases from P3 to P5 and P8 indicating ongoing regression, whereas in *Lrp5*$^{-/-}$ mice there is no significant change. Based on our understanding that regression of the ocular vessel networks is dependent on induced programmed cell death (Lang and Bishop, 1993; Diez-Roux and Lang, 1997), these data suggest that a reduced level of apoptosis is the cause of the persistence of the hyaloid vessels.

Discussion

Lrp5-deficient mice display two phenotypes: a low bone mass due to decreased bone formation and a persistent embryonic eye vascularization due to failed macrophage-mediated apoptosis. Several lines of evidence indicate that we have characterized the phenotypic consequences of a loss-of-function allele. First, there was no *Lrp5* expression detected by a 3′ probe in *Lrp5*$^{-/-}$ mice, indicating that no exon skipping has occurred. Second, although the allele is dominant for the bone mass abnormality, the phenotype in homozygotes is more severe than in heterozygotes. Third, the eye phenotype is recessive. Fourth, and most compelling, the phenotypes of *Lrp5*$^{-/-}$ mice are virtually identical to those observed in patients with a similar mutation as well as those lacking the entire LRP5 protein (Gong et al., 2001).

Lrp5 as a determinant of peak bone mass in vertebrates

Three aspects of osteoblast biology could be controlled by the Lrp5 signaling pathway: differentiation, proliferation, and function. The decreased number of bone marrow stromal cell progenitors may be viewed as a differentiation defect. However, the normal expression of *Cbfa1*, the earliest marker of osteoblast differentiation, and of *Osteocalcin*, the latest marker of osteoblast differentiation, together with the absence of any detectable phenotypic abnormalities in *Lrp5*$^{-/-}$ mice before birth, strongly suggest that the Lrp5

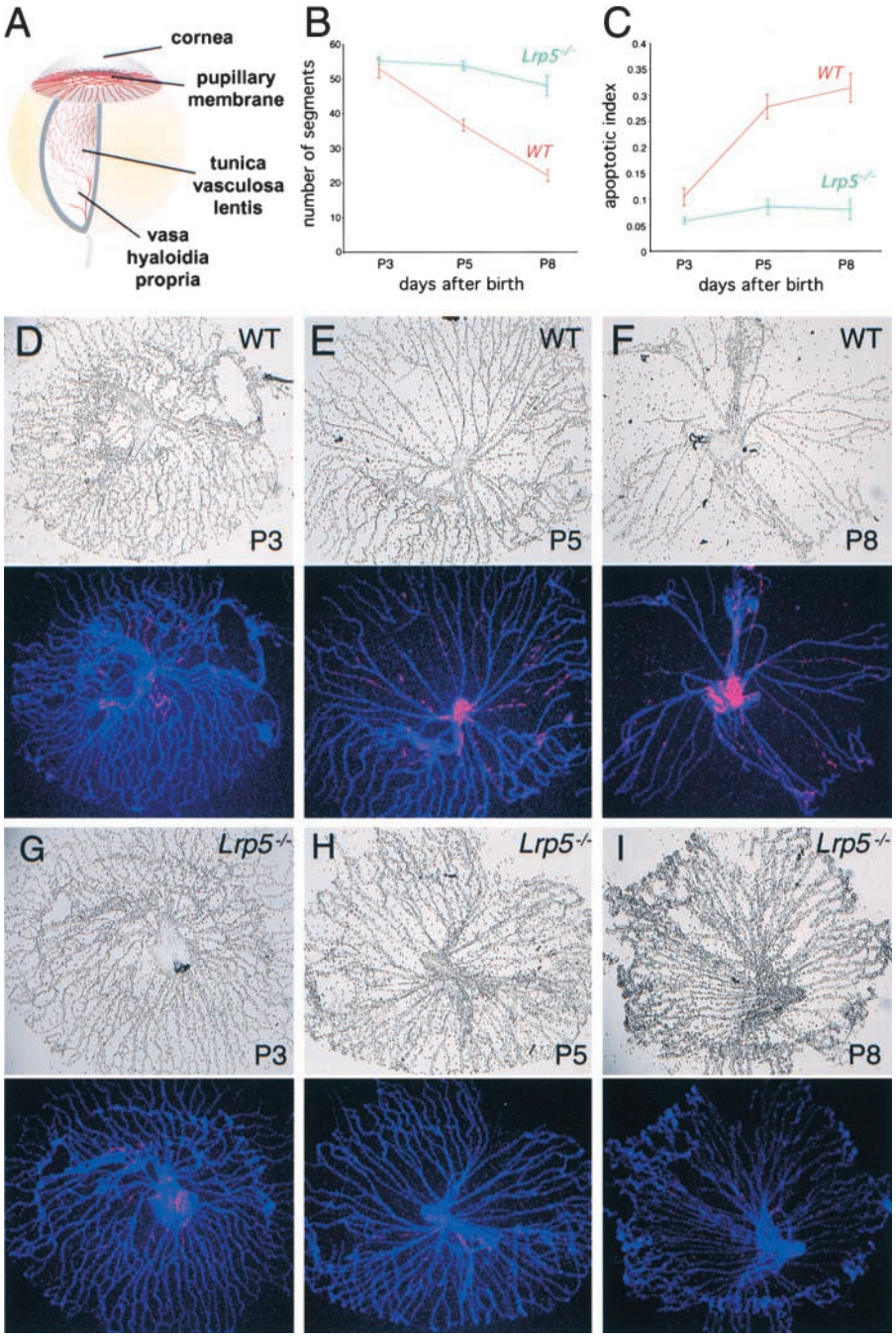

Figure 8. **Regression of hyaloid vessels is defective in *Lrp5*$^{-/-}$ mice.** (A) Schematic indicating the location of the temporary ocular capillary networks including the hyaloid vessels (vasa hyaloidia propria), the TVL and PM. (B) Quantification of the number of hyaloid vessels during a developmental time-course for wild-type (red line) and *Lrp5*$^{-/-}$ mice (green line). (C) Quantification of the apoptotic index (apoptotic capillary segments per total capillary segments) within the hyaloid vessels during a developmental time course for wild-type (red line) and *Lrp5*$^{-/-}$ mice (green line). Whole-mount preparations of hyaloid vessels for wild-type (D–F) and *Lrp5*$^{-/-}$ mice (G–I). Hyaloid vessel preparations are shown as pairs of brightfield and fluorescence images. Brightfield images are shown in the upper panel of each pair. In the lower panel, DAPI labeling of nuclei is shown in blue and apoptotic cell detection in red. The normal process of regression in wild-type hyaloid vessels is apparent (D to F) as is the lack of regression and a lower number of apoptotic capillary segments in *Lrp5*$^{-/-}$ hyaloid vessels (G to I). D–I are at 50× magnification.

signaling pathway does not play a major role in the process of Cbfa1-dependent osteoblast differentiation. Several lines of evidence suggest that the Lrp5 signaling pathway plays an important role in osteoblast proliferation. First, the total number of osteoblasts was decreased in the skeleton of *Lrp5*$^{-/-}$ mice compared with wild-type controls. Second, and more importantly, by in vivo BrdU labeling we observed a lower proportion of proliferating osteoblasts in *Lrp5*$^{-/-}$ mice than in wild-type controls. Third, the number of stromal cell progenitors was markedly reduced in the bone marrow of *Lrp5*$^{-/-}$ mice. These developmental defects are not the only ones observed in osteoblasts in the absence of *Lrp5*. Indeed, the reduction in the MAR in *Lrp5*$^{-/-}$ mice and the delay in mineralization observed in primary cultures of *Lrp5*$^{-/-}$ osteoblasts suggest that the function of differentiated osteoblasts, i.e., bone matrix deposition, is decreased in *Lrp5*$^{-/-}$ mice.

Together, these two abnormalities lead to the inability of *Lrp5*$^{-/-}$ mice to reach a normal bone mass early during life. The bone mass normally achieved early on in vertebrate life, also called peak bone mass, has been shown to be genetically controlled (Johnston and Slemenda, 1993). Our data are consistent with the hypothesis that the Lrp5 signal transduction pathway is one of the genetic determinants of peak bone mass in vertebrates.

Uncovering a Cbfa1-independent control of osteoblast biology

Our findings, together with those of Gong et al. (2001) and Little et al. (2002), have two implications. First, the observa-

tion that Lrp5 signaling is important for osteoblast proliferation and bone formation suggests an additional, postnatal function for the Wnt proteins in skeletal biology. However, we are aware that despite the interaction between Wnt1 and Lrp5 reported here, the Wnt proteins may not be the only class of secreted molecules transducing their signals through Lrp5. This is an important concern, as other Lrps have been shown to have multiple ligands (Herz and Strickland, 2001).

Second, *Lrp5* disruption reveals the existence of an additional, evolutionarily conserved, pathway besides Cbfa1-dependent gene expression, for controlling osteoblast proliferation and bone formation. The normal expression of *Cbfa1* in *Lrp5*$^{-/-}$ mice implicates other transcriptional mediators in this alternate pathway. Because Lef/Tcf proteins are well characterized transcriptional mediators of Wnt actions in other organ systems (Merrill et al., 2001) and are expressed in osteoblasts, one or more members of this family are likely to control some aspects of osteoblast biology. An important question in bone biology will now be to define which aspects of bone biology are affected by Wnt and Lef/Tcf proteins and how these functions relate to Lrp5 function.

Wnt proteins and postnatal bone formation

Cell culture analyses have shown that LRP5 acts as a coreceptor for Wnt proteins (Mao et al., 2001). Our analysis defines this interaction as being one of direct binding and demonstrates its biological importance in vivo. We also observed expression of *Wnt*, *Frizzled*, *β-catenin*, and *Tcf* genes in osteoblasts. The decreased expression of *Lef1* in *Lrp5*$^{-/-}$ osteoblasts suggests that *Lef1* expression is controlled directly or indirectly by the Lrp5 signaling pathway, and that Lef1 may be the preferred transcriptional effector of the various functions of this pathway in osteoblasts.

What may be the Wnt protein(s) that control osteoblast proliferation and function? The absence of *Wnt3a* expression in any bone sample analyzed implies that it is not the ligand of Lrp5 in bone. The accelerated ossification caused by *Wnt4* overexpression in chick limb buds (Hartmann and Tabin, 2000) is the mirror image of the bone phenotype of *Lrp5*$^{-/-}$ mice. To our surprise, DNA cotransfection experiments showed that Wnt1, but not Wnt4, induces Lef1-dependent gene expression. Wnt proteins have been separated into two categories based on their ability to induce dorsal axis duplication in *Xenopus* embryos. Members of the Xwnt8 family induce axis duplication, whereas members of the Xwnt5a do not. In that respect, it is interesting to note that Wnt1 belongs to the first family, whereas Wnt4 belongs to the second family (Wodarz and Nusse, 1998). The function of Wnt1 itself during skeletal development and during bone formation has not been reported, in part because Wnt1-deficient mice die shortly after birth (McMahon and Bradley, 1990). This question can now be addressed by a conditional gene inactivation strategy. The identification of the ligand(s) for Lrp5 is an urgent need in the field of bone biology.

Lrp5 requirement during eye development

The mammalian eye is vascularized during embryonic development with three connected but anatomically distinct networks: the PM, TVL, and hyaloid vessels (Fig. 8 A). In the mouse, all three networks regress postnatally due to apoptosis of capillary cells (Lang et al., 1994; Meeson et al., 1996; Lang, 1997; Ito and Yoshioka, 1999). *Lrp5*$^{-/-}$ mice have a reduced level of capillary cell apoptosis and a defect in hyaloid vessel regression resulting in the retention of the hyaloid vasculature throughout life. It has been shown previously that ocular macrophages found closely associated with these vascular networks are necessary and sufficient for the cell death that drives the regression process (Lang and Bishop, 1993; Diez-Roux and Lang, 1997; Lang, 1997). Lrp5 is produced by macrophages but is not detectable in endothelial cells, suggesting that Lrp5 has a crucial role to play in macrophage-induced capillary cell death.

The presence of normal numbers of ocular macrophages in *Lrp5*$^{-/-}$ mice indicates that Lrp5 is not critical for macrophage survival or migration. This raises the hypothesis that an Lrp5 ligand, perhaps a member of the Wnt family, is critical for macrophage function, and more specifically, for the killing action of macrophages. Although a precise understanding of the role of Lrp5 in programmed capillary regression will require further experimentation, this phenotype is of great interest because it indicates for the first time a signaling pathway that is required for macrophages to kill other cells in a developmental context. Even more intriguing is the possibility that this mouse model will lead us to an understanding of the means by which macrophage-mediated endothelial cell killing might be harnessed for therapeutic benefit in the treatment of diseases characterized by inappropriate angiogenesis.

Materials and methods

Lrp5 targeting and generation of *Lrp5*$^{-/-}$ mice

To generate a targeting vector, genomic clones containing exons 6–8 of *Lrp5* were isolated from a mouse 129/Sv genomic library. A replacement vector was constructed as follows: A PGK-neo cassette and IRES-β-galactosidase gene was inserted into an *Sph*I site in exon 6 (Fig. S1 A). The linearized vector was electroporated into embryonic stem (ES) (R1) cells, and after double selection by G418 and FIAU, *Lrp5*-targeted ES cell clones were identified by Southern blot hybridization using 5′ and 3′ flanking probes (Fig. S1 B). The ES cells carrying the correct mutation were injected into C57BL/6J blastocysts. Resulting male chimeras were mated to C57BL/6J females, and heterozygous offspring were identified by Southern blot hybridization. Northern blots were performed with 5 μg poly-A+ RNA (Fig. 1 B) or 1–10 μg total RNA (Figs. 1 C and 5 I) according to standard procedures. A 401-bp fragment from a *Pst*I and *BamH*I digestion of the *Lrp5* cDNA was used as a 5′ probe, located between nucleotide positions 71 (exon 1) and 471 (exon 2) of the *Lrp5* open reading frame. A 520-bp fragment from a *BamH*I and *Pst*I digestion of the *Lrp5* cDNA was used as a 3′ probe, located between nucleotide positions 2301 (exon 10) and 2821 (exon 12) of the *Lrp5* open reading frame.

Immunohistochemistry

Frozen sections were cut at 10 μm, and Lrp5 was detected with the AS884 murine-specific N-terminal antibody as previously described (Figueroa et al., 2000). Primary antibody was detected with an Alexa Fluor-594 chicken anti–rabbit secondary antibody (Molecular Probes). Anti-Cbfa1 antibody #770 was used to detect osteoblasts on alternate sections and detected with an anti–rabbit HRP secondary antibody (Santa Cruz Biotechnology), followed by detection with DAB (Vector Laboratories). Macrophages were identified using an F4/80 antibody (Serotec) followed by detection with an Alexa Fluor-647 chicken anti–rat secondary antibody (Molecular Probes). Sections were counterstained with Hoechst stain to visualize nuclei.

Morphological and histological analyses

Skeletons from pups were prepared as described (Kochhar, 1973) and stained with Alcian blue and Alizarin red. All mice were injected with calcein, 10 and 2 d prior to sacrifice (Vignery and Baron, 1980). Undecalci-

fied bones were fixed, dehydrated through an ethanol series, embedded in methylmethacrylate at 4°C, and 7-μm sections were prepared. Sections were stained with von Kossa reagent and counterstained by van Gieson reagent. Histomorphometric analysis was performed according to standard protocols (Parfitt et al., 1987) using the OsteoMeasure Analysis System (Osteometrics). Two sections from the third lumbar vertebra (L3) and two sections from L4 were measured for bone volume and tissue volume. All sections were >25 μm, i.e., more than one trabecular width apart. The mean distance between the calcein double labels was measured from 12-μm sections and used to calculate the MAR. These sections were also used to determine the mineralizing surface. Bone formation rate was calculated as the product of mineralizing surface per bone surface (Parfitt et al., 1987). Osteoblasts were counted separately in the primary and secondary spongiosa according to morphological criteria; cuboidal cells attached to bone occurring in clusters and having a large, asymmetrically positioned nucleus. The primary spongiosa was defined as the metaphyseal bone within one high power field (40× objective) of the growth plate. Statistical differences between groups were assessed by Student's *t* test.

Proliferation studies

Stromal cell progenitors were obtained by flushing bone marrow from 1–3-mo-old wild-type and *Lrp5*$^{-/-}$ mouse femora and tibiae. 0.5, 1.0, 2.0, and 4.0×10^7 nucleated cells were plated in 75-cm^2 flasks in αMEM/15% FBS, which was supplemented with 50 μg/ml ascorbic acid and fresh medium after 3 d of culture. The medium was then changed every 2 d with fresh ascorbic acid added until harvest at day 10–14. Colonies were stained for alkaline phosphatase activity as previously described (Ducy et al., 1999), and the experiment repeated three times (n = 5–8 mice per genotype per experiment). For in vivo BrdU labeling, 4-d-old mice were injected intraperitoneally with 100 μl of 100 μM BrdU in PBS, sacrificed 4 h later, calvaria were isolated, fixed for 6 h in 10% formalin in PBS and processed in paraffin. Sections of 5 μm were prepared and stained with the BrdU staining kit (Zymed). Apoptotic cells were detected in calvarial sections by measuring terminal transferase labeling of cells (DeadEnd; Promega). Eight animals per genotype were used and three sections per animal were studied. Statistical differences between groups were assessed by Student's *t* test.

Cell culture, DNA transfection, Western blotting, and immunoprecipitation

Primary osteoblast cultures from calvaria of newborn, wild-type, and *Lrp5*$^{-/-}$ mice were established and mineralized in vitro as previously described (Ducy et al., 1999). Transfections were performed in 24-well plates (20,000 cells/well; Fugene6; Roche) in triplicate and repeated at least three times; cells were harvested 40 h after transfection. Empty vector was added to keep the total amount of DNA constant at 225 ng/well. The FOPtkluc reporter, containing mutated Lef1 binding sites, was used in control transfections. All luciferase values were corrected for β-galactosidase activity as a control for transfection efficiency. For Western blot analysis, primary osteoblast lysates were collected in physiological buffer with protease inhibitor cocktail (Roche), homogenized, fractionated into cytosolic and membrane fractions by ultracentrifugation at 100,000 *g* for 90 min, and separated by SDS-PAGE. The epitope tags were detected by the anti-FLAG M2 antibody (Sigma-Aldrich) and anti-HA antibody (Santa Cruz Biotechnology). The anti–β-catenin antibody was obtained from Transduction Laboratories. Coimmunoprecipiation assay was performed using transfected COS-7 cells that were lysed with 400 μl of RIPA buffer (50 mM Tris/Cl, pH 8, 150 mM NaCl, 1% NP-40, 0.5% Na deoxycholate, 0.1% SDS) with protease inhibitor cocktail. After removing cell debris by brief centrifugation, 200 μl of cell lysate were incubated with 10 μg of anti-HA or anti-Flag antibody for 90 min. 25 μl of protein G Sepharose (Amersham Pharmacia Biotech) was added and incubated for 90 min. The Sepharose was washed three times, and precipitated proteins were separated by SDS-PAGE followed by Western blot analysis using the anti-Flag or anti-HA antibodies.

Gene expression analyses

Total RNA was isolated from calvaria, long bones stripped of bone marrow and primary osteoblasts from P4 wild-type and mutant mice using Trizol (Invitrogen), and treated with DNaseI (Invitrogen). Reverse transcription was performed on 4 μg of RNA using SuperscriptII (Invitrogen) according to the manufacturer's protocol. Reverse transcription reactions were amplified by PCR using gene-specific primers in standard reaction conditions with a 2-min initial denaturation step followed by 24 or 30 cycles of 94°C–20 s, 58°C–20 s, and 72°C–60 s. Reverse transcribed cDNA from day 11 embryos (E11) was used as a positive control for all PCR reactions. All products were resolved on a 1.6% agarose gel and analyzed by Southern blot hybridization using specific probes. PCR primers used for amplification are available upon request. RNase protection assays were performed on 5 μg total RNA (pretreated with DNaseI) using gel eluted probes prepared with the MAXIscript kit (Ambion). The RPAIII kit (Ambion) was used, products were separated on a 7.5% acrylamide gel and detected by autoradiography. The sizes of the full-length probes and protected fragments were confirmed using the RNA Century ladder (Ambion). The *Lef1* and *Tcf4* templates were those used for in situ hybridization analysis in Hartmann and Tabin (2000).

Preparation of hyaloid vessels, TUNEL labeling, and quantification

Animals were anesthetized, perfused with 4% PFA in PBS, eyeballs enucleated, and injected with a 1.5% solution of low melting point agarose in PBS. After 30 min at room temperature, eyeballs were incised around the equator. The hyaloid vessels embedded in agarose were removed from the retinal cup, heated on a glass slide, washed with PBS, and air dried; hyaloid vessel preparations were permeabilized with 0.05% Triton X-100 in PBS and processed for TUNEL labeling. Apoptotic cells were labeled using the DeadEnd kit (Promega) and visualized with streptavidin-Alexa Fluor 568 conjugate (Molecular Probes). Images were taken using Zeiss Axioplan microscope and a Sony DKC5000 digital camera. The total number of blood vessels and the number of TUNEL-labeled segments were quantified using established methods (Ito and Yoshioka, 1999) where we counted the number of vessels crossing a circle drawn at 50% of the maximum radial spread of the preparations. The apoptotic index was calculated as the ratio of the number of TUNEL-labeled vessels to the total number of blood vessels. At least three hyaloid vessel preparations were quantified for each time-point. Error bars represent standard errors.

Chemistry and hormone measurements

Calcium and phosphate were measured by their respective kits (Sigma-Aldrich). Deoxypyridinoline crosslinks were measured in morning urines using the Pyrilinks-D immunoassay kit (Metra Biosystems). Creatinine values were used for standardization between urine samples (Creatinine kit; Metra Biosystems) (n = 8 animals per genotype).

Online supplemental material

Online supplemental materials are available at http://www/jcb.org/cgi/content/full/200201089/DC1. Fig. S1 depicts the targeting strategy used for Lrp5, the Southern blot confirming correct targeting and genotyping data showing a normal Mendelian distribution at birth but slightly fewer animals (22.1%) alive at 1 mo of age. Fig. S2 shows a radiograph of a tibial fracture that occurred in a 2-mo-old Lrp5$^{2/2}$ mouse. Fig. S3 shows Western blots for the Wnt3a and Wnt4 transfection experiments to confirm expression and show cytoplasmic accumulation of β-catenin.

We are indebted to J. Aubin, C.P. Austin (Merck Research Laboratories, West Point, PA), H. Clevers (Utrecht University, Utrecht, Netherlands), P. Ducy, R. Grosschedl (University of Munich, Munich, Germany), J. Graff (University of Texas Southwestern, Dallas, Texas), K. Hirschi (Baylor College of Medicine, Houston, TX), T.J. Martin, J. Meeldijk, S. Nomura, J. Quinn, V. Shpacovitch, R. Smith, C. Tabin, and P. Younan for providing reagents, suggestions, and expert experimental help. We are grateful to P. Ducy for critical readings of the manuscript.

This work was supported by the following: March of Dimes (FY99-489); National Institutes of Health (DK58882, AR42919, and DE11290 to G. Karsenty, and HL51586 and HL16512 to L. Chan); a grant from the Societe Française de Rhumatologie; a grant from the Philippe Fondation (R. Levasseur); and a Canadian Institutes of Health Research Fellowship (M.S. Patel).

Submitted: 22 January 2002
Revised: 19 February 2002
Accepted: 5 March 2002

References

Aaron, J.E., N.B. Makins, R.M. Francis, and M. Peacock. 1984. Staining of the calcification front in human bone using contrasting fluorochromes in vitro. *J. Histochem. Cytochem.* 32:1251–1261.

Bhanot, P., M. Brink, C.H. Samos, J.C. Hsieh, Y. Wang, J.P. Macke, D. Andrew, J. Nathans, and R. Nusse. 1996. A new member of the frizzled family from *Drosophila* functions as a Wingless receptor. *Nature.* 382:225–230.

Brown, S.D., R.C.J. Twells, P.J. Hey, R.D. Cox, E.R. Levy, A.R. Soderman, M.L. Metzker, C.T. Caskey, J.A. Todd, and J.F. Hess. 1998. Isolation and charac-

terization of LRP6, a novel member of the low density lipoprotein receptor gene family. *Biochem. Biophys. Res. Commun.* 248:879–888.

Diez-Roux, G., and R.A. Lang. 1997. Macrophages induce apoptosis in normal cells in vivo. *Development.* 124:3633–3638.

Dong, Y., W. Lathrop, D. Weaver, Q. Qiu, J. Cini, D. Bertolini, and D. Chen. 1998. Molecular cloning and characterization of LR3, a novel LDL receptor family protein with mitogenic activity. *Biochem. Biophys. Res. Commun.* 251: 784–790.

Ducy, P., M. Starbuck, M. Priemel, J. Shen, G. Pinero, V. Geoffroy, M. Amling, and G. Karsenty. 1999. A Cbfa1-dependent genetic pathway controls bone formation beyond embryonic development. *Genes Dev.* 13:1025–1036.

Figueroa, D.J., J.F. Hess, B. Ky, S.D. Brown, V. Sandig, A. Hermanowski-Vosatka, R.C. Twells, J.A. Todd, and C.P. Austin. 2000. Expression of the type I diabetes-associated gene LRP5 in macrophages, vitamin A system cells, and the Islets of Langerhans suggests multiple potential roles in diabetes. *J. Histochem. Cytochem.* 48:1357–1368.

Gavrieli, Y., Y. Sherman, and S.A. Ben-Sasson. 1992. Identification of programmed cell death in situ via specific labeling of nuclear DNA fragmentation. *J. Cell Biol.* 119:493–501.

Gong, Y., M. Vikkula, L. Boon, J. Liu, P. Beighton, R. Ramesar, L. Peltonen, H. Somer, T. Hirose, B. Dallpiccola, et al. 1996. Osteoporosis-pseudoglioma syndrome, a disorder affecting skeletal strength and vision, is assigned to chromosome region 11q12-13. *Am. J. Hum. Genet.* 59:146–151.

Gong, Y., R.B. Slee, N. Fukai, G. Rawadi, S. Roman-Roman, A.M. Reginato, H. Wang, T. Cundy, F.H. Glorieux, D. Lev, et al. 2001. LDL receptor-related protein 5 (LRP5) affects bone accrual and eye development. *Cell.* 107:513–523.

Hartmann, C., and C.J. Tabin. 2000. Dual roles of Wnt signaling during chondrogenesis in the chicken limb. *Development.* 127:3141–3159.

Hartmann, C., and C.J. Tabin. 2001. Wnt-14 plays a pivotal role in inducing synovial joint formation in the developing appendicular skeleton. *Cell.* 104: 341–351.

Herz, J., and Y. Beffert. 2000. Apolipoprotein E receptors: linking brain development and Alzheimer's disease. *Nat. Rev. Neuroscience.* 1:51–58.

Herz, J., and D.K. Strickland. 2001. LRP: a multifunctional scavenger and signaling receptor. *J. Clin. Invest.* 108:779–784.

Hey, P.J., R.C.J. Twells, M.S. Phillips, Y. Nakagawa, S.D. Brown, Y. Kawaguchi, R. Cox, G. Xie, V. Dugan, H. Hammond, et al. 1998. Cloning of a novel member of the low-density lipoprotein receptor family. *Gene.* 216:103–111.

Huelsken, J., and W. Birchmeier. 2001. New aspects of Wnt signaling pathways in higher vertebrates. *Curr. Opin. Genet. Dev.* 5:543–553.

Hussian, M.M., D.K. Strickland, and A. Bakillah. 1999. The mammalian low-density lipoprotein receptor family. *Annu. Rev. Nutr.* 19:141–172.

Ishii, H., S.-H. Kim, T. Fujita, Y. Endo, S. Saeki, and T. Yamamoto. 1998. cDNA cloning of a new low-density lipoprotein receptor-related protein and mapping of its gene (LRP3) to chromosome bands 19q12-q13.2. *Genomics.* 51: 132–135.

Ito, M., and M. Yoshioka. 1999. Regression of the hyaloid vessels and pupillary membrane of the mouse. *Anat. Embryol.* 200:403–411.

Johnston, C.C., and C.W. Slemenda. 1993. Determinants of peak bone mass. *Osteoporos. Int.* 1:S54–S55.

Karsenty, G. 1999. The genetic transformation of bone biology. *Genes Dev.* 13: 3037–3051.

Kim, D.-H., Y. Inagaki, T. Suzuki, R.X. Ioka, S.Z. Yoshioka, K. Moagoori, M.-J. Kang, Y. Cho, A.Z. Nakano, Q. Liu, et al. 1998. A new low density lipoprotein receptor related protein, LRP5, is expressed in hepatocytes and adrenal cortex, and recognized apolipoprotein E. *J. Biochem.* 124:1072–1076.

Kochhar, D.M. 1973. Limb development in mouse embryos. Analysis of teratogenic effects of retinoic acid. *Teratology.* 7:289–298.

Korinek, V., N. Barker, P.J. Morin, D. van Wichen, R. de Weger, K.W. Kinzler, B. Vogelstein, and H. Clevers. 1997. Constitutive transcriptional activation by a beta-catenin-Tcf complex in APC−/− colon carcinoma. *Science.* 275: 1784–1787.

Lang, R.A. 1997. Apoptosis in mammalian eye development: lens morphogenesis, vascular regression and immune privilege. *Cell Death Differ.* 4:12–20.

Lang, R.A., and M.J. Bishop. 1993. Macrophages are required for cell death and tissue remodeling in the developing mouse eye. *Cell.* 74:453–462.

Lang, R.A., M. Lustig, F. Francois, M. Sellinger, and H. Plesken. 1994. Apoptosis during macrophage-dependent tissue remodelling. *Development.* 120:3395–3403.

Little, R.D., J.P. Carulli, R.G. Del Mastro, J. Dupuis, M. Osborne, C. Folz, S.P. Manning, P.M. Swain, S.C. Zhao, B. Eustace, et al. 2002. A mutation in the LDL receptor-related protein 5 gene results in the autosomal dominant high-bone-mass trait. *Am. J. Hum. Genet.* 70:11–19.

Mao, J., J. Y. Wang, L. Bo, W. Pan, G.H. Farr, III, C. Flynn, H. Yuan, S. Takada, D. Kimelman, L. Lin, and D. Wu. 2001. Low-density lipoprotein receptor-related protein-5 binds to axin and regulates the canonical Wnt signaling pathway. *Mol. Cell.* 7:801–809.

McMahon, A.P., and A. Bradley. 1990. The Wnt-1 (int-1) proto-oncogene is required for development of a large region of the mouse cell. *Cell.* 62:1073–1085.

Meeson, A., M. Palmer, M. Calfon, and R.A. Lang. 1996. A relationship between flow and apoptosis during programmed capillary regression is revealed by vital analysis. *Development.* 122:3929–3938.

Merrill, B.J., U. Gat, R. DasGupta, and E. Fuchs. 2001. Tcf3 and Lef1 regulate lineage differentiation of multipotent stem cells in skin. *Genes Dev.* 15: 1688–1705.

Parfitt, A.M., M.K. Drezner, F.H. Glorieux, H.A. Kanis, H. Malluche, P.J. Meunier, S.M. Ott, and R.R. Recker. 1987. Bone histomorphometry: standardization of nomenclature, symbols, and units. report of the ASBMR histomorphometry committee. *J. Bone Miner. Res.* 6:595–610.

Parr, B.A., and A.P. McMahon. 1998. Sexually dimorphic development of the mammalian reproductive tract requires Wnt-7a. *Nature.* 95:707–710.

Perrimon, N., and A.P. McMahon. 1998. Negative feedback mechanisms and their roles during pattern formation. *Cell.* 97:707–710.

Pinson, K.I., J. Brennan, S. Monkley, B.J. Avery, and W.C. Skarnes. 2000. An LDL-receptor-related protein mediates Wnt signalling in mice. *Nature.* 407: 535–538.

Shibamoto, S., K. Kigano, R. Takada, F. Ito, M. Takeichi, and S. Takada. 1998. Cytoskeletal reorganization by soluble Wnt-3a protein signalling. *Genes Cells.* 3:659–670.

Superti-Furga, A., B. Steinmann, and F. Perfumo. 1986. Osteoporosis-pseudoglioma or osteogenesis imperfecta? *Clin. Genet.* 2:185–185.

Tamai, K., M. Semenov, Y. Kato, R. Spokony, C. Liu, Y. Katsuyama, F. Hess, J.P. Saint-Jeannet, and X. He. 2000. LDL-receptor-related proteins in Wnt signal transduction. *Nature.* 407:530–535.

Tomita, Y., D.-H. Kim, K. Magoori, T. Fujino, and T.T. Yamamoto. 1998. A novel low-density lipoprotein receptor-related protein with type II membrane protein-like structure is abundant in heart. *J. Biochem.* 124:784–789.

Vainio, S., M. Heikkila, A. Kispert, N. Chin, and A.P. McMahon. 1999. Female development in mammals is regulated by Wnt-4 signalling. *Nature.* 397: 405–409.

Vignery, A., and R. Baron. 1980. Dynamic histomorphometry of alveolar bone remodeling in the adult rat. *Anat. Rec.* 196:191–200.

Wehrli, T.E. 1999. The low-density lipoprotein receptor gene family: multiple roles in lipid metabolism. *J. Mol. Med.* 77:306–315.

Willnow, T.E. 1999. The low-density lipoprotein receptor gene family: multiple roles in lipid metabolism. *J. Mol. Med.* 77:306–315.

Wodarz, A., and R. Nusse. 1998. Mechanisms of Wnt signaling in development. *Annu. Rev. Cell Dev. Biol.* 14:59–88.

Yamazaki, H., H. Bujo, J. Kusunoki, K. Seimiya, T. Kanaki, N. Morisaki, W.J. Schneider, and Y. Saito. 1996. Elements of neural adhesion molecules and a yeast vacuolar protein sorting receptor are present in a novel mammalian low density lipoprotein receptor family member. *J. Biol. Chem.* 271:24761–24768.